

Growth and Fabrication of Quasivertical Current Aperture Vertical Electron Transistor Structures

Philipp Doering,* Rachid Driad, Stefano Leone, Stefan Mueller, Patrick Waltereit, Lutz Kirste, Vladimir Polyakov, Michael Mikulla, and Oliver Ambacher

The current aperture vertical electron transistor (CAVET) combines the high carrier mobility of the AlGaIn/GaN heterostructure with the better electric field distribution of the vertical topology, allowing for higher power densities if compared with lateral high electron mobility transistors (HEMTs). The formation of a current blocking layer (CBL), without degenerating the aperture region and the subsequently overgrown AlGaIn/GaN heterostructure is the key building block of such devices. Herein, a comparison of GaN:Mg nonplanar selective area growth (SAG) and Mg-ion implantation is carried out primarily focusing on structural evolution, Mg distribution, and 2D electron gas (2DEG) performance. The epitaxial growth process in SAG is correlated to local growth increase and ridge development, and then optimized regarding mesa filling. AlGaIn/GaN regrowth is analyzed regarding structural evolution after overgrowth and Mg distribution into the GaN channel. Considerably lower Mg-distribution into subsequently grown layers is detected for implanted samples in agreement with the electrical performance of the overgrown AlGaIn/GaN heterostructures. A GaN-on-Si quasivertical CAVET structure with an Mg-implanted CBL and 250 nm channel thickness is fabricated. High surface quality and proper 2DEG performance demonstrate the potential use of GaN-on-Si CAVET's using Mg implantation for CBL fabrication.


1. Introduction

GaN-based devices offer great potential for high-power and high-frequency applications. Nevertheless, most investigated lateral high electron mobility transistor (HEMT) structures suffer from high gate-to-drain spacing to sustain high voltage/high current operation. Vertical topologies have been shown to have the potential to overcome these limitations.^[1–5] The current aperture vertical electron transistor (CAVET) has been proven to be a promising candidate for vertical GaN devices due to low specific on-resistance and dispersion free transistors.^[6] However, GaN substrates used for CAVETs, are still expensive and small in size, making alternative substrate materials more attractive for mass production. Especially, quasi- and fully vertical GaN-on-Si transistors are of great interest as a cost effective and high scalable alternative to bulk GaN substrates. Remarkable results have been already demonstrated in metal-oxide semiconductor field effect transistor (MOSFET) technology,

showing blocking voltages of over 800 V.^[7,8] On the contrary, despite the high potential of GaN-on-Si CAVETs, such structures were not reported yet. A CAVET combines the high mobility and carrier density of the AlGaIn/GaN heterostructure with the high packaging density of the vertical topology. In analogy to the double diffused metal-oxide semiconductor field effect transistor (DMOS) structure in Si technology, a current blocking layer (CBL) provides a potential barrier for electrons between the source and drain contact and serves as a current guide through the aperture region. The peak electric field is buried in the bulk material contrary to lateral HEMT avoiding surface-related breakdown.^[9] A major challenge in the fabrication of CAVETs is the formation of such CBL, while preserving a high quality of the aperture region. The very thin channel in the final device structure and the resulting low distance between the doped CBL and the 2D electron gas (2DEG) requires a high quality in surface morphology after preparing the CBL by local doping. In addition, the doping distribution during subsequent overgrowth needs to be limited, to ensure proper 2DEG performance. In the past, ion implantation^[10] and selective area growth (SAG) using metalorganic chemical vapor deposition (MOCVD) and molecular beam epitaxy (MBE)^[11] were conducted to create the CBL. It was shown

P. Doering, Prof. O. Ambacher
INATECH – Department of Power Electronics
Albert-Ludwigs University Freiburg
Emmy-Noether-Str. 2, Freiburg 79108, Germany
E-mail: philipp.doering@inatech.uni-freiburg.de

Dr. R. Driad, Dr. S. Leone, S. Mueller, Dr. P. Waltereit, Dr. L. Kirste,
Dr. V. Polyakov, Dr. M. Mikulla, Prof. O. Ambacher
Fraunhofer IAF
Fraunhofer Institute for Applied Solid State Physics
Tullastraße 72, Freiburg 79108, Germany

 The ORCID identification number(s) for the author(s) of this article can be found under <https://doi.org/10.1002/pssa.202000379>.

© 2020 The Authors. Published by Wiley-VCH GmbH. This is an open access article under the terms of the Creative Commons Attribution-NonCommercial-NoDerivs License, which permits use and distribution in any medium, provided the original work is properly cited, the use is non-commercial and no modifications or adaptations are made.

Correction added on 30 September 2020, after first online publication: Projekt Deal funding statement has been added.

DOI: 10.1002/pssa.202000379

that both types of process flows can potentially be used for CAVET fabrication. Earlier research in SAG in GaN focused primarily on dislocation density reduction by epitaxial lateral overgrowth (ELO)^[12] and its related techniques.^[13–15] Originally, nonplanar SAG in (Al)GaN technology was introduced with a focus on buried ridge laser diodes,^[16] aiming to provide an electrical and optical guide. More recently, this technique received further attention on the regrowth of contact layers, to reduce contact resistance and thermal budget to the heterostructures, as compared with annealing processes for contact development via Si implantation.^[17–19] The attempt for a CAVET differs widely due to subsequent overgrowth by an AlGaN/GaN structure, which is highly sensitive to its underground. In particular, the background doping^[20] of the channel and the morphology^[21] of the aimed device structure need to be controlled precisely. However, there is no detailed study on the epitaxial growth on CBL via selected area growth of GaN:Mg and the influence on the subsequent overgrowth of AlGaN/GaN. In this study, a full MOCVD-based approach on quasivertical CAVETs on silicon and sapphire substrates is presented, using nonplanar SAG and ion implantation to form the CBL. A comparison of both potential fabrication techniques is carried out with special attention to structural evolution, doping distribution during overgrowth, and the influence on the 2DEG performance of the final heterostructures.

2. Device Layout and Process Flow

The total thickness of GaN layers on silicon substrates is generally limited due to the high lattice mismatch and the difference in thermal expansion coefficient.^[22,23] The uid-GaN (unintentionally doped) drift layer in a quasivertical structure with a standard strain management, using a step grade AlGaN buffer, is also limited in thickness to avoid cracking and excessive bowing issues. In our structure, a 1.2 μm uid-GaN drift layer and a 300 nm GaN:Mg CBL were used. A 300 nm n^+ -GaN drain contact for the quasivertical setup was buried between the AlGaN buffer and the drift layers. The current aperture had a width of 10 μm . The dimension of the gate contact was chosen to result in 2 μm gate-aperture overlap to ensure accurate gate control.^[9] A 250 nm uid-GaN channel was deposited, due to best trade-off characteristics between on-state resistance, source leakage, and potential interference with the p-type-doped CBL.^[11] The resulting current distribution of such a device was simulated using a self-consistent Poisson-solver and is shown in **Figure 1**.

The fabrication of a CAVET requires a regrowth process in any case regardless of the used process flow. In this work, the aperture region is first grown by MOCVD. Afterward, the CBL is defined by either SAG or ion implantation, as shown in **Figure 2**. In the case of SAG, the wafers are masked to define an aperture region by mesa etching. To fill up these mesas, a subsequent epitaxial regrowth is performed, resulting in the formation of a CBL adjacent to the undoped aperture region. No etching is necessary in the case of ion implantation. Nevertheless, both types of process flows require a subsequent overgrowth of the GaN channel and the AlGaN barrier to finalize the device structure.

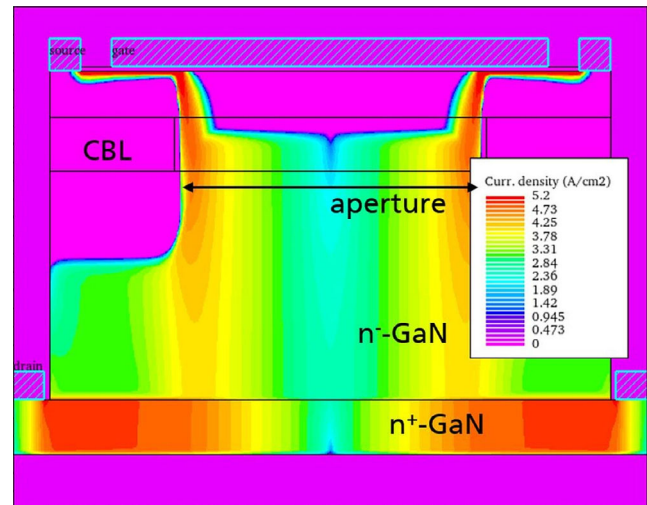


Figure 1. 2D current distribution in a quasivertical CAVET structure. Aperture width = 10 μm ; GaN-channel thickness = 250 nm; Gate-aperture overlap = 2 μm . Drain contact layer thickness = 300 nm. Drift layer thickness = 1.2 μm .

3. CBL Formation

GaN templates were grown by MOCVD on sapphire substrates with a 0.9 μm -thick Fe-compensated GaN layer followed by a 2 μm unintentionally doped GaN layer. All templates had a sheet resistance of $>80 \text{ k}\Omega \square^{-1}$. A $\text{SiO}_x/\text{Si}_x\text{N}_y$ dielectric mask ($\approx 220 \text{ nm}$; deposited by plasma-enhanced chemical vapor deposition) was then used for the chlorine-based dry etching process of mesas with a depth of around 350 nm. The root mean square (RMS) of the etched samples were in the same range as the templates after growth (RMS $\approx 0.4 \text{ nm}$ in a $10 \times 10 \mu\text{m}^2$ scan). The same dielectric mask was used for the subsequent SAG of the p-CBL. MOCVD growth pressure and temperature were varied at the beginning of deposition, to investigate the impact of the growth regime on the filling of the mesas and the surface morphology close to the masked area. A V/III ratio of 3200 was used in all of the analyzed growth conditions. Optimized mesa filling was observed at low pressure of 50 mbar and 1030 $^\circ\text{C}$ surface temperature. As the pressure was increased to 200 mbar, a modest roughening was noted close to the masked area. Scanning electron microscopy (SEM) images, shown in **Figure 3**, revealed that the filling of the mesa is not entirely completed, yet. Particularly, areas with low filling factor (low ratio of masked to unmasked area) revealed that the mesa have not been completely closed by SAG. Holes in the epitaxial layer were noticeable, thus they gradually decrease by increasing the distance from the dielectric mask. A starting 3D-growth mode clearly dominated at high growth pressure of 400 mbar leading to increased roughening and island-style growth adjacent to the dielectric mask. Only partial nucleation sites seemed to occur in thinner stripes, probably as result of lower adatom mobility. The degradation of the crystalline quality seemed to be limited to the area very close to the dielectric mask. The remaining layer did not show any surface roughening, similar to the reference wafers without any dielectric mask for all pressure regimes. We used the low-pressure regime at 50 mbar to investigate the effect of

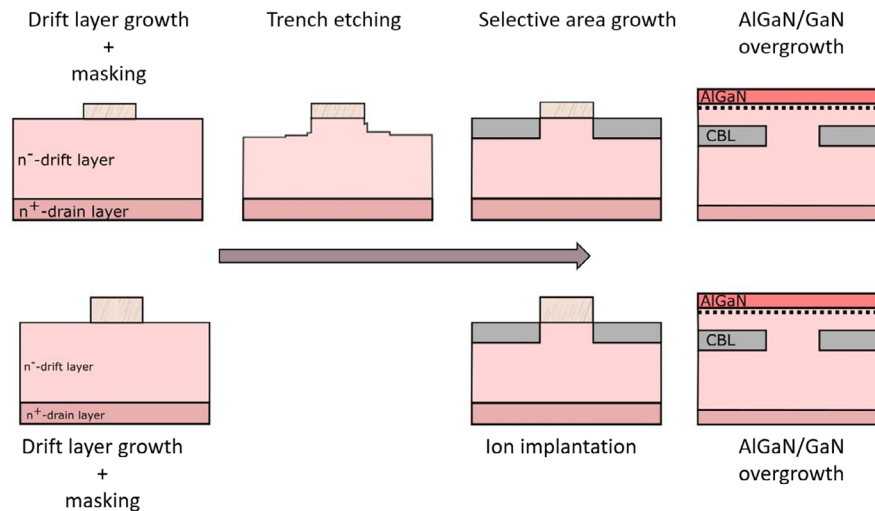


Figure 2. Process flow of the fabricated CAVET structures in this work. The upper part shows the CBL formation by mesa etching and subsequent nonplanar SAG. The lower part illustrates the formation of the CBL by ion implantation. Both structures are finished by planar regrowth of an AlGaIn/GaN heterostructure.

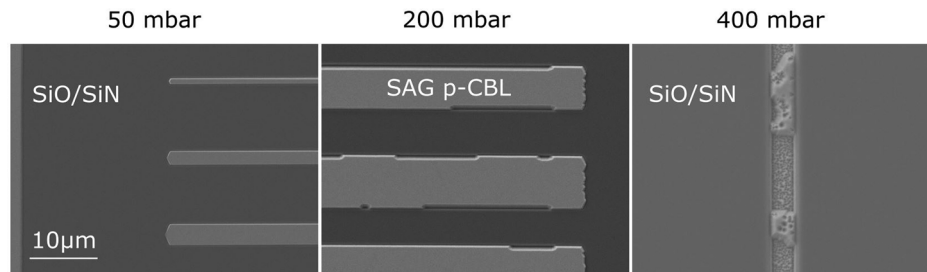


Figure 3. Scanning electron microscopy images of the SAG growth at 50 (left), 200 (center), and 400 mbar (right). With increasing pressure, a clear degradation of the mesa filling is observable. At high growth pressure (400 mbar), only partial nucleation occurs in etched structures between the SiO/SiN dielectric mask.

temperature on SAG. A pronounced effect was only noted for high growth temperatures of 1070 °C, as the morphology of the regrown GaN layers clearly degraded. Moreover, the morphological change was not restricted to areas close to the dielectric mask or with low filling factor but for the whole layer. Degradation resulting from low growth temperature (990 °C) was only slightly visible. Regardless of the applied growth regime, a ridge developed close to the masked area. Due to the excessive amount of adatoms, the growth rates close to the mesa region increased massively when compared with the regions in far distance to the dielectric mask. To investigate the ridge development atomic force microscopy (AFM) profiling on stripes with 45 μm length and 10 μm width was conducted (Figure 4a). Cross-sections along *m*-direction [1-100] and *a*-direction [11-20] have been carried out, as shown in Figure 4b. The growth rates and the widths of developed ridges in dependence on the applied growth regime are shown in Figure 4c,d, respectively. In all cases, the grown layers had a growth rate far away from masked areas between 0.60 and 0.68 μm h⁻¹. A local increase in the growth rate at the ridges from 1.10 to 1.55 μm h⁻¹ is observed with decreasing pressure and from 1.28 to 1.61 μm h⁻¹ with decreasing temperature. In contrast to a decreasing growth rate, the ridge width increased with growth temperature and pressure. In addition, the ridges showed

a symmetrical shape along *m*-plane [1-100] as reported by Heikmann et al.^[24] but had an asymmetrical character along *a*-plane [11-20] probably as a result of the off-cut of the sapphire substrate. For the alternative CAVET structures, Mg implantation with an energy of 100 keV at 7° off-cut to form the p-CBL was also investigated. A low implant dose of $2 \times 10^{14} \text{ cm}^{-2}$ was applied to prevent the amorphization of the implanted layer. First, equivalent GaN-on-sapphire templates were taken as a direct comparison with the CAVET structures obtained by SAG. A second set of GaN templates were later grown on silicon substrates using an AlGaIn step graded buffer to reduce lattice mismatch-induced strain. A 300 nm GaN:Ge drain contact layer was deposited followed by an 1.2 μm uid-GaN drift layer, similar to the simulated CAVET structure. The aperture regions were protected by a 3 μm-thick photoresist. The Mg-implanted layers were analyzed by AFM and Nomarski differential interference contrast (NDIC) microscopy before and after implantation, but a morphological change was not observed on neither of the substrates.

4. AlGaIn/GaN Overgrowth

Concerning the final CAVET structure, the issue of Mg diffusion at high growth temperatures^[25] needs to be addressed, to prevent

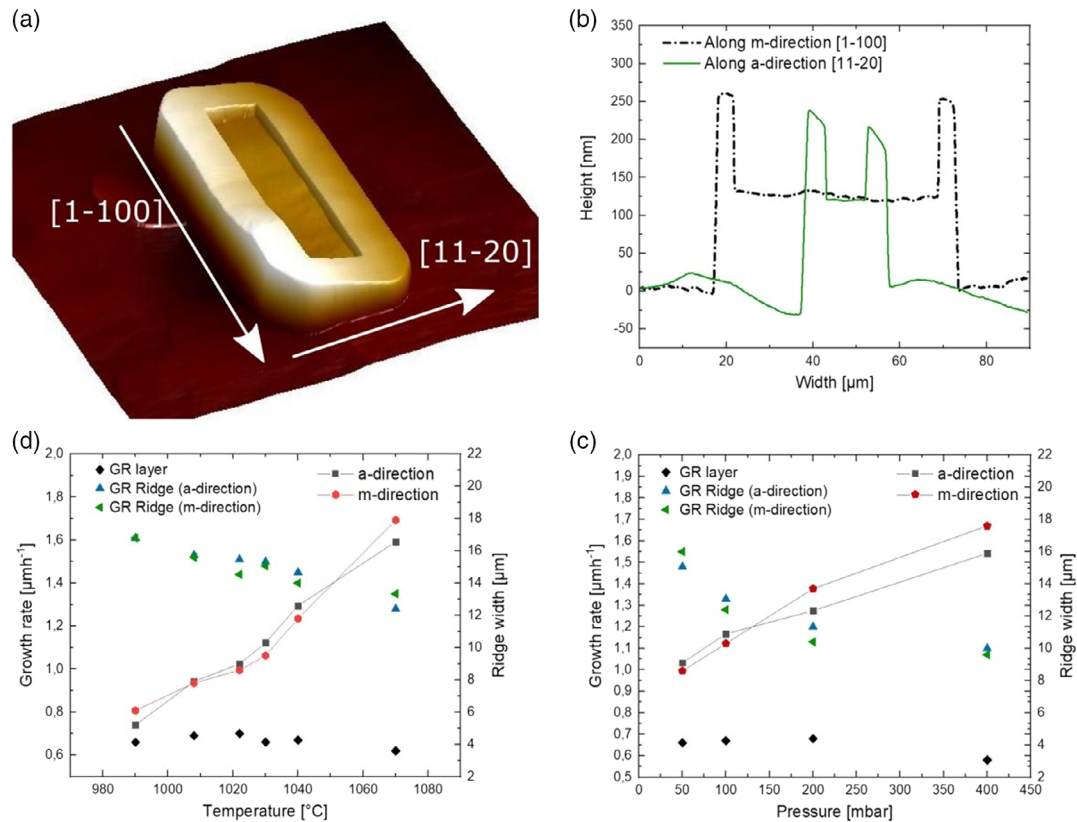


Figure 4. a) 3D schematic of the resulting ridge of the nonplanar SAG obtained using Bruker's NanoScope Analysis software; b) corresponding cross-section along *a*- [11-20] and *m*-directions [1-100] of the ridge; the flat part in the center corresponds to the dielectric mask; c) growth rate and ridge width as a function of temperature; d) growth rate and ridge width in dependence on pressure.

dopant distribution to the vicinity of the barrier channel interface. An interference with the 2DEG would significantly limit the device performance due to compensation of carriers by Mg acceptors. In a first set of experiments, to evaluate the electrical performance of AlGaIn/GaN heterostructures, test structures were overgrown on Mg-doped (samples A, B, and C) and Mg-implanted (D) templates on sapphire substrates. Prior to overgrowth, sample A was submitted to a buffered hydrofluoric acid (BHF) solution for 2 min, to remove the Mg-enriched surface layer. Sample B had an additional oxygen plasma treatment prior to BHF etching as done for sample A. Sample C was overgrown without any pretreatment. A supplemental sample (E) without a Mg-doped layer served as a reference sample. All samples had a channel thickness of 500 nm. The electrical characteristics of the regrown heterostructures and their surface morphology are shown in Table 1. The heterostructures deposited on samples with Mg doping by MOCVD (A–C), show a considerable degradation in the electrical performance in comparison with the implanted (D) and the reference sample (E). On the contrary, surface morphology and quality does not seem to be a crucial element contributing to electrical degradation as an increase in surface roughness or change in morphological characteristics was not observable. However, secondary ion mass spectroscopy (SIMS) measurements revealed a perceivably different Mg distribution between samples B, C, and D, as shown in

Table 1. Electrical characteristics of AlGaIn/GaN on sapphire substrates on Mg-doped samples.

Sample ^{a)}	R_{SEDDY} [Ω □ ⁻¹]	R_{SHALL} [Ω □ ⁻¹]	μ [cm ² Vs ⁻¹]	n_{SHEET} [cm ⁻²]	RMS ^{b)} [nm]
A (BHF)	2370	1940	591	8.1×10^{12}	0.56
B (O ₂ + BHF)	1800	1644	839	4.5×10^{12}	0.54
C (as grown)	19 400	n.a. ^{a)}	n.a. ^{a)}	n.a. ^{a)}	0.63
D (Mg impl.)	502	455	896	1.3×10^{13}	0.84
E (reference)	410	407	1080	1.2×10^{13}	0.53

^{a)}High resistance, no ohmic behavior; ^{b)} $10 \times 10 \mu\text{m}^2$ scan.

Figure 5. As the Mg decay was nearly identical to sample B, sample A is neglected in this figure. To mark the regrowth interface (RI), we included the Si signal of the reference sample. Si enriched GaIn interfaces are a commonly observed feature of regrowth.^[26,27] The acidic treatment of Mg-doped layers with diluted hydrofluoric acid (HF) or BHF, was shown to be an effective removal of the Mg-rich surface, reducing segregation effects.^[28] In our case, a positive impact was also noticed, which is consistent with the aforementioned electrical characteristics, as the Mg concentration seemed to drop earlier after the RI. However, a faster decay rate of the Mg profile, as mentioned

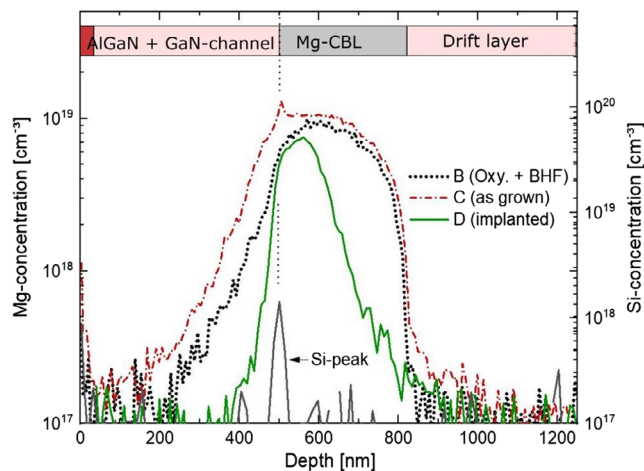


Figure 5. SIMS depth profile of Mg distribution after AlGaIn/GaN overgrowth for the sample B, C, D, and the Si signal of sample E (equivalent to the RI).

in the study by Xing et al.,^[28] was not observed. A considerably sharper Mg profile was perceived for sample D with a decay rate of 40 nmdec^{-1} in the range of 5×10^{18} – $5 \times 10^{17} \text{ cm}^{-3}$. The fast decay of the Mg concentration resulting in better separation from the 2DEG matched with the significantly improved electrical results. The measured sheet resistance of $455 \Omega \square^{-1}$ (Hall measurement in van der Pauw geometry) was only slightly higher if compared with the reference sample ($407 \Omega \square^{-1}$). The slightly lower mobility of sample D is probably attributed by the increase in RMS and sheet carrier density, when compared with sample E. As a second step, the test structures were replicated on conductive silicon substrates, as described in Section 3. The channel thickness was reduced to 250 nm, as in the proposed device structure in Section 2. High-resolution X-ray diffraction (HRXRD) analysis revealed an Al content of 23%, a barrier thickness of 24 nm, and a GaN cap thickness of 3 nm. The capacitance–voltage (CV) profile and the conductance divided by the angular frequency (G/ω) of the resulting HEMT structure on the Mg-implanted layer is shown in **Figure 6**. A depletion was

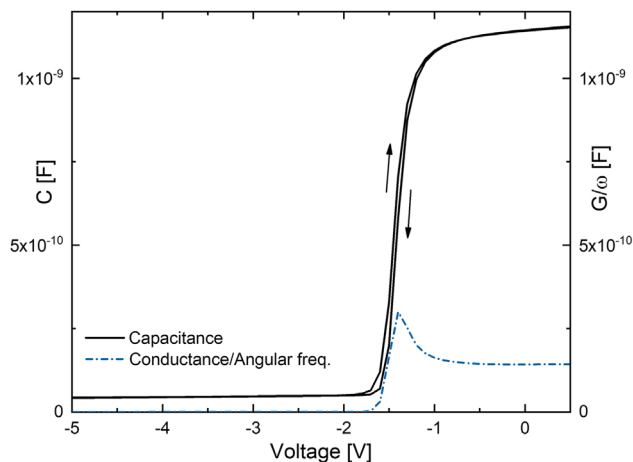


Figure 6. C–V and G/ω –V profiles of a HEMT structure with 250 nm GaN-channel on Mg-implanted layer.

observable in addition to a negligible hysteresis of the forward and backward measurements. The peak of the G/ω , solely resulting from the displacement and depletion of the interface states,^[29] confirmed the presence of the 2DEG. A sheet carrier density of $4.8 \times 10^{12} \text{ cm}^{-2}$ was derived from the CV profile as described by Ambacher et al.^[21] A surface roughness of 0.49 nm was measured by a $10 \times 10 \mu\text{m}^2$ scan. Similar electrical and morphological results were obtained for the reference structure on uid-GaN-on-Si structures. To even further decrease the Mg distribution into the overgrown layer, the growth temperature of the GaN channel was reduced from 1000 to 900 °C. However, no significant improvement of the Mg decay was observed. CV measurements did not show any depletion in the measured range, in contrast to the heterostructures grown on implanted Mg layers. Finally, the AlGaIn/GaN overgrowth was replicated on selectively implanted and selective regrown Mg-doped samples on silicon and sapphire substrates, respectively. As described earlier, no morphological change was observed for the derived CAVET-structures fabricated via Mg implantation in comparison with the reference wafers. A surface roughness of around 0.6 nm was obtained by AFM (**Figure 7b**), independent of the measured wafer position. In contrast, the morphological trend of the ridge development remained for CAVET structures obtained via SAG. **Figure 7c,d** shows the NDIC image of a CAVET structure after AlGaIn/GaN overgrowth. The surface morphology, due to the ridge around the dielectric mask used in the nonplanar SAG, was preserved after the overgrowth of the channel and barrier layer. AFM analyses showed, that surface steps of larger than 100 nm were measurable as a result of SAG. These ridge-like structures were shown in the past to limit the breakdown voltage in CAVETs.^[9,11] This was explained by the local conductivity increase close to the masked area occurring for Si-containing dielectrics as a result of autodoping^[24] and due to an increase in impurity incorporation due to the growth on inclined facets after dry etching.^[30]

5. Conclusion

The growth and fabrication of quasivertical CAVET structures were investigated regarding structural evolution, Mg doping distribution, and electrical performance of an overgrown AlGaIn/GaN heterostructure. At low growth pressure, nonplanar SAG achieved the most promising results. However, regardless of the growth regime, a ridge with an asymmetrical character along *a*-plane was observed. About 2.5 times higher local growth rates were derived from AFM measurements because of the excessive amount of adatoms close to the dielectric mask. A correlation between ridge width, local growth rate, and applied growth regime was shown. Mg distribution during AlGaIn/GaN overgrowth was determined by SIMS measurements. A positive effect of HF pretreatment was observable with considerably sharper doping profiles for Mg-implanted samples. The observations were in good agreement with the electrical results obtained by Eddy-current and Hall measurements, whereas no significant difference in sheet resistance was observed for Mg-implanted samples. HEMT-structures on Mg-doped samples showed an increase in sheet resistance as a result of Mg diffusion or segregation. CV measurements revealed proper 2DEG behavior for

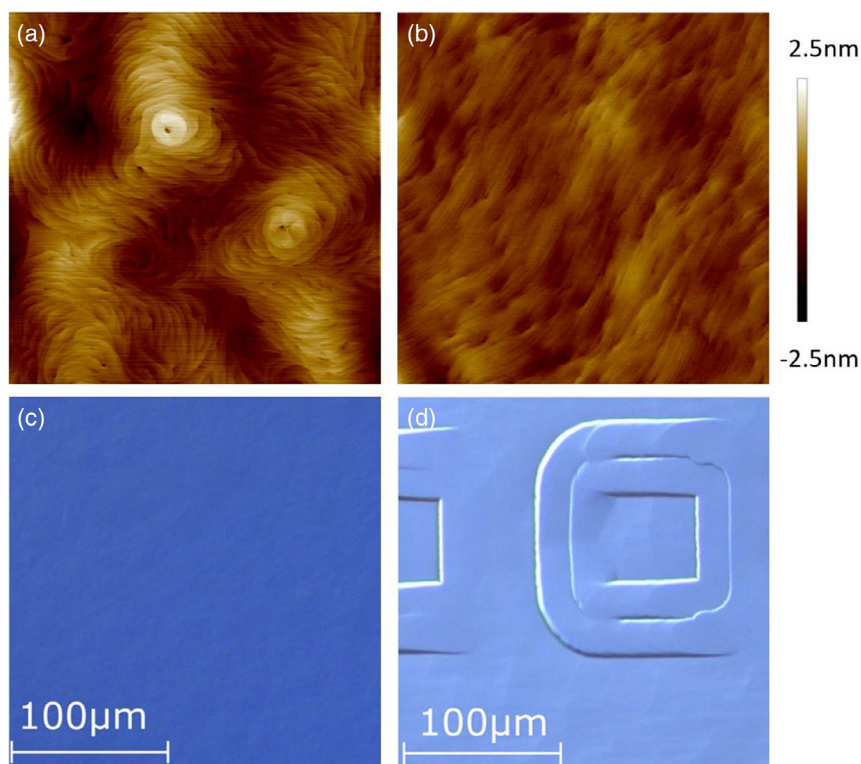


Figure 7. a) A $10 \times 10 \mu\text{m}^2$ AFM image of a HEMT structure on Mg-implanted GaN-on-Si; b) $10 \times 10 \mu\text{m}^2$ AFM image of a HEMT structure on nonplanar SAG p-GaN on sapphire; c) NDIC image of a regrown AlGaIn/GaN structure on Mg-implanted GaN-on-Si; d) NDIC image of a round CAVET structure of a regrown HEMT structure on nonplanar SAG p-GaN on sapphire.

AlGaIn/GaN HEMTs on conductive silicon substrates overgrown after Mg implantation. The final planar overgrowth on structured samples showed, that the morphology of the selectively regrown samples was preserved. On the contrary, AlGaIn/GaN overgrowth on Mg-implanted structures did not show any surface degradation regardless of the analyzed position on the wafer.

6. Experimental Section

The epitaxial growth process was carried out in two different MOCVD reactors, one with a horizontal stream and one with a vertical gas stream. Standard precursors for nitride semiconductor growth were used for the supply of nitrogen (ammonia— NH_3), gallium (trimethylgallium—TMGa), and aluminum (trimethylaluminum—TMAI). A mixture of nitrogen and hydrogen was supplied as carrier gas. Bis(cyclopentadienyl)magnesium (Cp_2Mg), bis(cyclopentadienyl)iron (Cp_2Fe), and isobutylgermane ($\text{C}_4\text{H}_9\text{Ge}$) were used as dopants to attain Mg, Fe, and Ge doping, respectively. A 3" sapphire with a thickness of 560 μm and 100 mm silicon with a thickness of 800 μm served as substrates for the epitaxial growth.

Surface morphology was evaluated by NDIC and AFM in tapping mode. Mesa filling of the SAG-regrown samples was supplementary analyzed by SEM with 5 kV acceleration voltage at different scanning angles. To detect the Mg and Si distribution of the samples described in this work, SIMS was used. SIMS profiling was recorded using 5 keV Cs primary ions at an imping angle of 45° and detecting MgCs^+ and SiCs^+ secondary ions. Relative sensitivity factors (RSFs) were used for quantitative calibration of the secondary ions with $\text{RSF} = C_M/(I_M/I_{\text{ref}})$. C_M is the concentration of the element (Mg or Si) and I_M and I_{ref} are the secondary-ion intensity of the element (Mg or Si) and the secondary-ion intensity of a reference sample. HRXRD measurements were carried out using Cu $\text{K}\alpha_1$ radiation with a two-bounce Ge 220 monochromator and a triple axis Ge 220 analyzer setup

to determine AlGaIn barrier and GaN cap thickness and the Al content of the barrier and crystalline quality. CV measurements were carried out by a mercury probe setup. An operating alternating current (AC) voltage of 50 mV at 10 kHz was applied. Forward (+ to −) and backward (− to +) measurements were carried out subsequently between +0.5 and −5 V. The conductance was directly divided by the angular frequency, which results in the same dimension as for the capacitance.^[31] The sheet resistance was measured by a Leighton Eddy-current measurement system and by Hall measurements in van der Pauw geometry. Hall measurements were also used to determine the sheet carrier density and the carrier mobility.

Acknowledgements

The authors thank all the colleagues at Fraunhofer IAF who have helped in the material preparation, characterization, and wafer processing. The authors thank especially Theo Fuchs providing SIMS measurements and Mario Prescher for HRXRD analysis. Thanks also to Dr. Klaus Köhler and Jana Ligl for fruitful discussion. Open access funding enabled and organized by Projekt DEAL.

Conflict of Interest

The authors declare no conflict of interest.

Keywords

current aperture vertical electron transistors, gallium nitride, ion implantations, nonplanar selective area growths

Received: June 22, 2020
Revised: August 14, 2020
Published online:

- [1] D. Ji, A. Agarwal, H. Li, W. Li, S. Keller, S. Chowdhury, *IEEE Electron Device Lett.* **201839**, 863.
- [2] D. Shibata, R. Kajitani, M. Ogawa, K. Tanaka, S. Tamura, T. Hatsuda, M. Ishida, T. Ueda, in *2016 IEEE Int. Electron Devices Meeting (IEDM)*, IEEE, San Francisco, CA **2016**, pp. 10.1.1–10.1.4.
- [3] T. Oka, T. Ina, Y. Ueno, J. Nishii, in *Proc. 28th Int. Symp. on Power Semiconductor Devices and ICs (ISPSD)*, The Japan Society of Applied Physics, Tokyo **2016**, pp. 459–462.
- [4] T. Oka, T. Ina, Y. Ueno, J. Nishii, *Appl. Phys. Express* **2015**, *8*, 54101.
- [5] D. Ji, C. Gupta, S. H. Chan, A. Agarwal, W. Li, S. Keller, U. K. Mishra, S. Chowdhury, in *2017 IEEE Int. Electron Devices Meeting (IEDM)*, IEEE, San Francisco, CA **2017**, pp. 9.4.1–9.4.4.
- [6] S. Chowdhury, M. H. Wong, B. L. Swenson, U. K. Mishra, *IEEE Electron Device Lett.* **2012**, *33*, 41.
- [7] C. Liu, R. Abdul Khadar, E. Matioli, *IEEE Electron Device Lett.* **2018**, *39*, 71.
- [8] R. A. Khadar, C. Liu, R. Soleimanzadeh, E. Matioli, *IEEE Electron Device Lett.* **2019**, *40*, 443.
- [9] I. Ben-Yaacov, Y.-K. Seck, U. K. Mishra, S. P. DenBaars, *J. Appl. Phys.* **2004**, *95*, 2073.
- [10] S. Chowdhury, B. L. Swenson, M. H. Wong, U. K. Mishra, *Semicond. Sci. Technol.* **2013**, *28*, 74014.
- [11] R. Yeluri, J. Lu, C. A. Hurni, D. A. Browne, S. Chowdhury, S. Keller, J. S. Speck, U. K. Mishra, *Appl. Phys. Lett.* **2015**, *106*, 183502.
- [12] T. S. Zheleva, O.-H. Nam, M. D. Bremser, R. F. Davis, *Appl. Phys. Lett.* **1997**, *71*, 2472.
- [13] A. Usui, H. Sunakawa, A. Sakai, A. A. Yamaguchi, *Jpn. J. Appl. Phys.* **1997**, *36*, L899.
- [14] K. Hiramatsu, K. Nishiyama, A. Motogaito, H. Miyake, Y. Iyechika, T. Maeda, *Phys. Status Solidi A* **1999**, *176*, 535.
- [15] T. S. Zheleva, S. A. Smith, D. B. Thomson, K. J. Linthicum, P. Rajagopal, R. F. Davis, *J. Electronic. Mater.* **1999**, *28*, L5.
- [16] M. Yang, M. Cho, C. Kim, J. Yi, J. Jeon, S. Khym, M. Kim, Y. Choi, S.-J. Leem, Y.-H. Lee, *J. Cryst. Growth* **2001**, *226*, 73.
- [17] S. Leone, P. Brueckner, L. Kirste, P. Doering, T. Fuchs, S. Mueller, M. Prescher, R. Quay, O. Ambacher, *Phys. Status Solidi B* **2019**, *257*, 1900436.
- [18] J. Guo, Y. Cao, C. Lian, T. Zimmermann, G. Li, J. Verma, X. Gao, S. Guo, P. Saunier, M. Wistey, D. Jena, H. G. Xing, *Phys. Status Solidi A* **2011**, *208*, 1617.
- [19] I. Milosavljevic, K. Shinohara, D. Regan, S. Burnham, A. Corrion, P. Hashimoto, D. Wong, M. Hu, C. Butler, A. Schmitz, P. J. Willadsen, M. Micovic, in *68th Device Research Conf.*, IEEE, South Bend, IN **2010**, pp. 159–160.
- [20] O. Ambacher, V. Cimalla, *Polarization Effects in Semiconductors*, Springer Science + Business Media LLC, Boston, MA **2008**.
- [21] O. Ambacher, J. Smart, J. R. Shealy, N. G. Weimann, K. Chu, M. Murphy, W. J. Schaff, L. F. Eastman, R. Dimitrov, L. Wittmer, M. Stutzmann, W. Rieger, J. Hilsenbeck, *J. Appl. Phys.* **1999**, *85*, 3222.
- [22] H. Amano, Y. Baines, E. Beam, M. Borga, T. Bouchet, P. R. Chalker, M. Charles, K. J. Chen, N. Chowdhury, R. Chu, C. de Santi, M. M. de Souza, S. Decoutere, L. Di Cioccio, B. Eckardt, T. Egawa, P. Fay, J. J. Freedman, L. Guido, O. Häberlen, G. Haynes, T. Heckel, D. Hemakumara, P. Houston, J. Hu, M. Hua, Q. Huang, A. Huang, S. Jiang, H. Kawai, et al., *J. Phys. D: Appl. Phys.* **2018**, *51*, 163001.
- [23] D. Marcon, B. de Jaeger, S. Halder, N. Vranckx, G. Mannaert, M. van Hove, S. Decoutere, *IEEE Trans. Semicond. Manufact.* **2013**, *26*, 361.
- [24] S. Heikman, S. Keller, S. P. DenBaars, U. K. Mishra, F. Bertram, J. Christen, *Jpn. J. Appl. Phys.* **2003**, *42*, 6276.
- [25] K. Köhler, R. Gutt, J. Wiegert, L. Kirste, *J. Appl. Phys.* **2013**, *113*, 73514.
- [26] J. Tajima, T. Hikosaka, M. Kuraguchi, S. Nunoue, *J. Cryst. Growth* **2019**, *509*, 129.
- [27] G. W. Pickrell, A. M. Armstrong, A. A. Allerman, M. H. Crawford, K. C. Cross, C. E. Glaser, V. M. Abate, *J. Electronic. Mater.* **2019**, *48*, 3311.
- [28] H. Xing, D. S. Green, H. Yu, T. Mates, P. Kozodoy, S. Keller, S. P. DenBaars, U. K. Mishra, *Jpn. J. Appl. Phys.* **2003**, *42*, 50.
- [29] E. H. Nicollian, A. Goetzberger, *Bell Syst. Techn. J.* **1967**, *46*, 1055.
- [30] S. C. Cruz, S. Keller, T. E. Mates, U. K. Mishra, S. P. DenBaars, *J. Cryst. Growth* **2009**, *311*, 3817.
- [31] K. Köhler, W. Pletschen, B. Godejohann, S. Müller, H. P. Menner, O. Ambacher, *J. Appl. Phys.* **2015**, *118*, 205702.